Journal of the Korean Physical Society (2023) 82:507–514
https://doi.org/10.1007/s40042-023-00706-z

Online ISSN 1976-8524
Print ISSN 0374-4884

REVIEW - PARTICLES AND NUCLEI

Exclusive photo- and electroproduction of vector mesons off protons

Sang-Ho Kim[1]

Received: 29 August 2022 / Accepted: 6 September 2022 / Published online: 12 January 2023

Abstract
We review the recent progress in the exclusive photo- and electroproduction of vector mesons off protons. The key experimental results from the CLAS, GlueX, and LEPS Collaborations are shown and compared with the theoretical calculations.

Keywords Photoproduction · Electroproduction · Effective Lagrangians · Regge model · GPD model

1 Introduction

Exclusive photoproduction of vector mesons provides substantial contributions to the spectroscopy of hadrons. For example, the photoproduction of strange vector mesons is valuable to gain a deep understanding of baryon resonances [1] and to search for the missing resonances which are predicted by a quark model but not observed yet experimentally [2]. An effective Lagrangian approach and a Regge model [3–8] are widely used to describe the available data (e.g., CLAS [9–12], CBELSA/TAPS [13], and LEPS [14] Collaborations) for the reactions $\gamma p \to K^*\Lambda$ and $\gamma p \to K^*\Sigma$. The cross-sections of these reactions are not much suppressed relative to those of kaon photoproduction [15–19], indicating that K^* channel is essential in the coupled-channel analyses for the study of baryon resonances.

The diffractive scattering processes $\gamma p \to Vp$, where V = (ρ^0 [20, 21], ω [22–24], ϕ [25–30], J/ψ [31, 32]), also have their own interest. They are governed by Pomeron exchange at high energies [33]. The gradually rising cross-section with the center-of-mass (c.m.) photon energy W is described by Pomeron exchange. Additional ingredients such as meson exchange in the t channel and N^* exchange in the s channel are necessary to account for the low energy data and a relevant theory capable of identifying N^* resonances and extracting the corresponding resonance parameters is called for. Note that, in case of ϕ and J/ψ photoproduction, because of the Okubo–Zwieg–Iizuka (OZI) rule [34–36], meson or N^* exchanges are highly suppressed relative to those of ρ^0 and ω photoproduction.

Exclusive electroproduction of ρ^0 [37–40], ω [41–43], and ϕ [44–47] light vector mesons enables us to understand the transition between the hadronic and partonic domains of the Quantum Chromodynamics (QCD) theory according to the ranges of the photon energy W and the photon virtuality Q^2. Extending to this virtual-photon sector offers a way to understand the hadronic properties of the virtual photon and to examine to what extent of W and Q^2 meson exchange is applicable. Figure 1 shows the graphical representations of the (a) t-channel meson exchange and of (b) handbag diagram for $\gamma^* p \to (\rho^0, \omega, \phi)p$. A hadronic Regge model is successful when going from photoproduction to low W and Q^2 ranges of electroproduction (Fig. 1a). Meanwhile, the handbag diagram of Fig. 1b takes over high ranges of W and Q^2. In such a hard scattering mechanism, the transition $\gamma_L^* \to V_L$ dominates the process and the generalized parton distributions (GPD) and factorization of scales become relevant.

In this article, we first review recent studies of exclusive photoproduction of K^* vector meson as well as ρ^0, ω, ϕ, and J/ψ ones. An effective Lagrangian approach is emphasized and its theoretical framework is explained in detail. The key experimental results are shown in comparison with the theoretical calculations. The Pomeron-exchange model is explained in some detail for the diffractive scattering processes $\gamma p \to (\rho^0, \omega, \phi, J/\psi)p$. We focus on the $\gamma p \to (\phi, J/\psi)p$ reaction and also discuss the possible existence of the pentaquark states $P_s^+(P_c^+)$ via the $\phi(J/\psi)$ photoproduction. Second, we review the studies of exclusive electroproduction of light vector mesons $\gamma^* p \to (\rho^0, \omega, \phi)p$. We show previous and current experiments in view of the

✉ Sang-Ho Kim
sangho.kim@ssu.ac.kr

[1] Department of Physics and Origin of Matter and Evolution of Galaxies (OMEG) Institute, Soongsil University, Seoul 06978, Korea

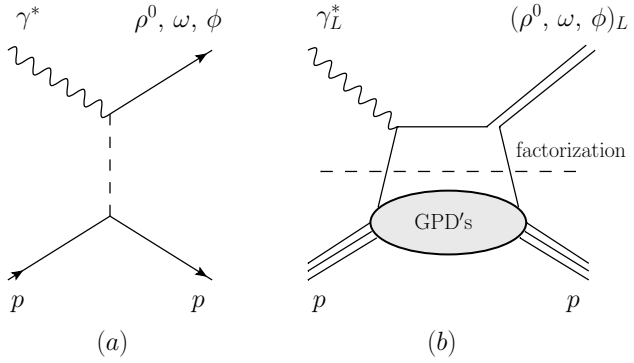

Fig. 1 Graphical representations of **a** the t-channel meson exchange and of **b** the handbag diagram for exclusive vector-meson electroproduction

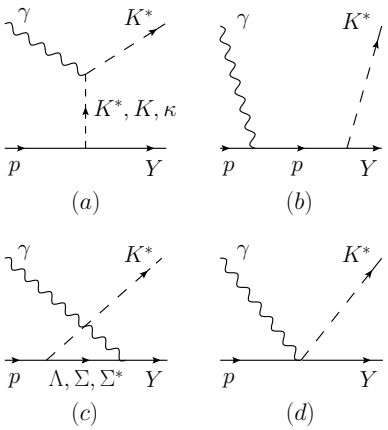

Fig. 2 Feynman diagrams for $\gamma p \to K^* Y$, where $Y = (\Lambda, \Sigma)$, are drawn for the exchanges of **a** strange mesons in the t channel, **b** proton in the s channel, and **c** hyperons in the u channel. **d** The contact term should be included for the charged K^* production to satisfy the gauge invariance

kinematical range of Q^2 and x_B and explain two relevant theoretical approaches. We also introduce other reaction processes where a GPD model is applicable.

This article is organized as follows. In Sect. 2, exclusive photoproduction of vector mesons is reviewed. Electroproduction of vector mesons is discussed in Sect. 3. The summary is given in Sect. 4.

2 Photoproduction of vector mesons

2.1 Production of K^* vector mesons

The Born diagrams for the strangeness production $\gamma p \to K^* Y$, where $Y = (\Lambda, \Sigma)$, are drawn in Fig. 2. The exchanges of (a) strange mesons in the t channel, (b) proton in the s channel, and (c) hyperons in the u channel are considered. (d) The contact term should be included for the charged K^* production to satisfy the gauge invariance.

An effective Lagrangian approach is employed in Ref. [3]. The photon interaction Lagrangians of strange mesons are given by

$$\begin{aligned}
\mathcal{L}_{\gamma K^* K^*} =& -ie_{K^*} A^\mu \left(K^{*\nu} K^{*\dagger}_{\mu\nu} - K^*_{\mu\nu} K^{*\dagger\nu} \right), \\
\mathcal{L}_{\gamma K K^*} =& g_{\gamma K K^*} \epsilon^{\mu\nu\alpha\beta} \left(\partial_\mu A_\nu \right) \left(\partial_\alpha K^*_\beta \right) K + \text{H.c.}, \\
\mathcal{L}_{\gamma \kappa K^*} =& g_{\gamma \kappa K^*} A^{\mu\nu} \kappa K^*_{\mu\nu} + \text{H.c.}.
\end{aligned} \tag{1}$$

The Lagrangians for the electromagnetic (EM) interactions of baryons are written by

$$\begin{aligned}
\mathcal{L}_{\gamma NN} =& -\bar{N} \left[e_N \gamma_\mu - \frac{e\kappa_N}{2M_N} \sigma_{\mu\nu} \partial^\nu \right] A^\mu N, \\
\mathcal{L}_{\gamma YY} =& \frac{e\kappa_Y}{2M_N} \bar{Y} \sigma_{\mu\nu} \partial^\nu A^\mu Y.
\end{aligned} \tag{2}$$

The strong interaction Lagrangians of strange mesons are given by

$$\begin{aligned}
\mathcal{L}_{K^* NY} =& -g_{K^* NY} \bar{N} Y \left[\gamma_\mu - \frac{\kappa_{K^* NY}}{2M_N} \sigma_{\mu\nu} \partial^\nu \right] K^{*\mu} \\
&+ \text{H.c.}, \\
\mathcal{L}_{KNY} =& -ig_{KNY} \bar{N} \gamma_5 Y K + \text{H.c.}, \\
\mathcal{L}_{\kappa NY} =& -g_{\kappa NY} \bar{N} Y \kappa + \text{H.c.}.
\end{aligned} \tag{3}$$

Here, the coupling constants are determined using the experimental data if the decay modes are available [1] or by using the theoretical models, such as the SU(3) flavor symmetry and Nijmegen potentials [48, 49]. For example, $g_{\gamma K K^*}$ in Eq. (1) is obtained from the experimental data for the radiative decay $\Gamma_{K^* \to K\gamma}$, which leads to

$$g^c_{\gamma K K^*} = 0.254 \text{ GeV}^{-1}, \; g^0_{\gamma K K^*} = -0.388 \text{ GeV}^{-1}, \tag{4}$$

where the phases of them are fixed from a quark model. The values in Eq. (3) from the Nijmegen potentials (NSC97a) are given by

$$\begin{aligned}
&g_{K^* N\Lambda} = -4.26, \;\; g_{K^* N\Sigma} = -2.46, \\
&\kappa_{K^* N\Lambda} = 2.66, \;\; \kappa_{K^* N\Sigma} = -0.467, \\
&g_{KN\Lambda} = -13.4, \;\; g_{KN\Sigma} = 4.09, \\
&g_{\kappa N\Lambda} = -8.31, \;\; g_{\kappa N\Sigma} = -5.32.
\end{aligned} \tag{5}$$

It turns out that t-channel K exchange gives a dominant contribution, while the K^*-exchange contribution is tiny, for $K^{*+}\Lambda$ production [3]. Reference [4] suggests that the light κ meson with a mass around (600–900) MeV could play an important role for $K^{*0}\Sigma^+$ production, while it is

supplementary in $K^{*+}\Lambda$ production, from the results of the parity asymmetry defined by [50, 51]

$$P_\sigma \equiv \frac{d\sigma^N - d\sigma^U}{d\sigma^N + d\sigma^U} = 2\rho^1_{1-1} - \rho^1_{00}, \quad (6)$$

because K^* exchange is absent in $K^{*0}\Sigma^+$ production. Here, ρ's are the K^* density matrix elements and $d\sigma^N(d\sigma^U)$ stands for the cross-section from the natural (unnatural) parity exchanges. Then, the LEPS Collaboration [14] has confirmed that the parity asymmetry is positive at forward angles for $\gamma p \to K^{*0}\Sigma^+$ as depicted in Fig. 3, indicating that natural-parity exchange is a dominant process at forward angles and the exchange of $\kappa(800)$ scalar meson is indeed essential.

Some N^* resonances given in the Particle Data Group (PDG) strongly couple to the KY channel [1]. Thus it is reasonable to include their contributions in the s channel in $\gamma p \to K^*Y$ besides the background production mechanism of Fig. 2. A few N^* resonances are included in Refs. [5, 6] and are found to be crucial in $K^*\Lambda$ production, while N^* contributions be marginal in $K^*\Sigma$ production in Ref. [7]. Here the N^* couplings to K^*Y are taken from a quark model prediction [2]. Meanwhile, the CLAS data at the Jefferson Laboratory (JLab) on the differential cross-sections, spin-density matrices, and Λ recoil polarizations for $\gamma p \to K^{*+}\Lambda$ are fitted within the Bonn-Gatchina (BnGa) partial wave analysis [12]. The fitted total cross-section is displayed in Fig. 4. K exchange (blue dot-dashed) falls off as $\sqrt{s} = W$ increases because the t-channel exchange model behaves as $\sigma \sim s^{J-1}$, where J is the spin of the exchanged particle. $N(1895)1/2^-$ (red dashed) and $N(2100)1/2^+$ (green dotted) provide very significant contributions to $\gamma p \to K^{*+}\Lambda$. Table. 1 lists the branching ratios for $N^* \to K^*\Lambda$ extracted from Ref. [12]. For the $K^*\Sigma$ channel, more experimental data are required to extract the main N^* decay modes.

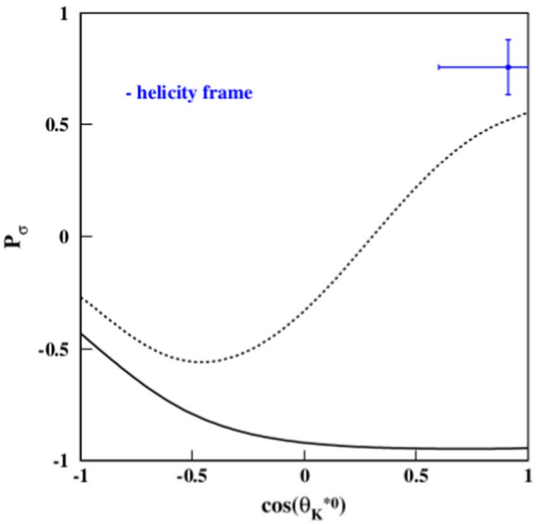

Fig. 3 Parity asymmetry versus $\cos\theta_{K^*}$ in the helicity frame from the LEPS Collaboration for $\gamma p \to K^{*0}\Sigma^+$ [14]. The data point is averaged over photon energies from 1.85 to 2.96 GeV. Solid curve is the result from Ref. [4] with almost no contribution from κ exchange, whereas dotted curve includes substantial κ exchange. Figure is taken from Ref. [14]

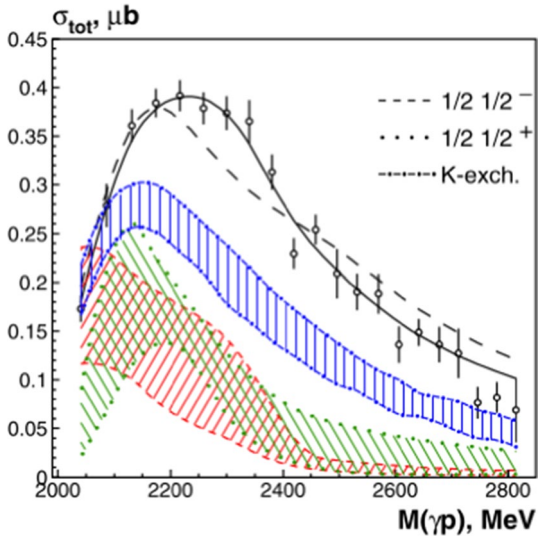

Fig. 4 Total cross-section versus beam energy W for $\gamma p \to K^{*+}\Lambda$ using the BnGa partial wave analysis [12]. The hatched regions are labeled above, and the solid curve represents the full BnGa fit. The dashed curve represents a fit which excludes the three high-mass resonances. The data are from the CLAS Collaboration [11]. Figure is taken from Ref. [12]

2.2 Production of ρ^0, ω, ϕ and J/ψ, vector mesons

The Born diagrams for the photoproduction of ρ^0, ω, ϕ, and J/ψ vector mesons are drawn in Fig. 5.

Table 1 N^* resonances and their branching ratios [%] to the K^*Y and VN decays given in the PDG [1], where $Y = (\Lambda, \Sigma)$ and $V = (\rho, \omega, \phi)$

PDG resonances	$K^*\Lambda$	$K^*\Sigma$	ρN	ωN	ϕN
$N(1875)3/2^-$ ***	< 0.2	–	36–56	15–25	–
$N(1880)1/2^+$ ***	0.5−1.1	–	19–45	12–28	–
$N(1895)1/2^-$ ****	4–9	–	14–50	16–40	–
$N(1900)3/2^+$ ****	< 0.2	–	25–40	7–13	–
$N(2000)5/2^+$ **	1–3	–	–	< 2	–
$N(2060)5/2^-$ ***	0.3−1.3	–	5–33	1–7	–
$N(2100)1/2^+$ ***	3–11	–	–	10–25	–
$N(2120)3/2^-$ ***	< 0.2	–	< 3	4–20	–
$N(2190)7/2^-$ ****	0.2−0.8	–	< 11	8–20	–

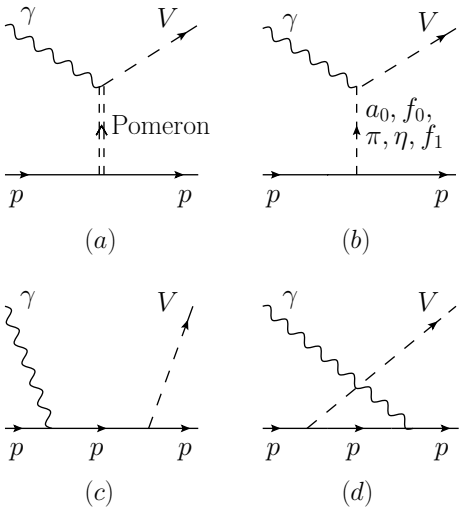

Fig. 5 Feynman diagrams for $\gamma p \to Vp$, where $V = (\rho^0, \omega, \phi, J/\psi)$, for the exchanges of **a** Pomeron, **b** light mesons in the t channel, and **c**, **d** proton in the s and u channels, respectively

The exchanges of (a) Pomeron, (b) light mesons in the t channel, and (c, d) proton in the s and u channels are considered. As for the two-gluon exchange of Fig. 5a, it is suggested by the Donnachie–Landshoff (DL) model [33, 52] that the Pomeron couples to the nucleon like a $C = 1$ isoscalar photon and its coupling is described in terms of the isoscalar EM form factor of the nucleon, $F_N(t)$. As a consequence, the Pomeron-exchange amplitude for $\gamma(q) + p(p_i) \to V(k) + p(p_f)$ can be written by

$$\mathcal{M}_{\mathbb{P}} = G_{\mathbb{P}}(s,t)\epsilon_\nu^* \mathcal{T}_{\mathbb{P}}^{\mu\nu}\epsilon_\mu, \tag{7}$$

where

$$\mathcal{T}_{\mathbb{P}}^{\mu\nu} = i\frac{12eM_V^2}{f_V}\beta_Q F_V(t)\beta_q F_N(t)\left(\gamma_\alpha q^\alpha g^{\mu\nu} - q^\nu\gamma^\mu\right), \tag{8}$$

with $t = (q-k)^2$. ϵ_μ and ϵ_ν stand for the polarization vectors of the incoming photon and outgoing vector meson, respectively. f_V is the vector-meson decay constant and is determined through the decay width of $\Gamma(V \to e^+e^-) = 4\pi M_V \alpha_{\rm em}/(3f_V^2)$ [1], which leads to $f_V = 4.94$, 17.06, 13.38, 11.18, and 39.68 for $V = \rho^0$, ω, ϕ, J/ψ, and $\Upsilon(1s)$ mesons, respectively. The coupling of the Pomeron with the quark Q (or the antiquark $\bar{Q}$) in the vector meson V is denoted by β_Q, while that with the light quark in the nucleon by β_q. The Pomeron–vector-meson vertex is dressed by the form factor

$$F_V(t) = \frac{1}{M_V^2 - t}\left(\frac{2\mu_0^2}{2\mu_0^2 + M_V^2 - t}\right), \tag{9}$$

and $F_N(t)$ is given by

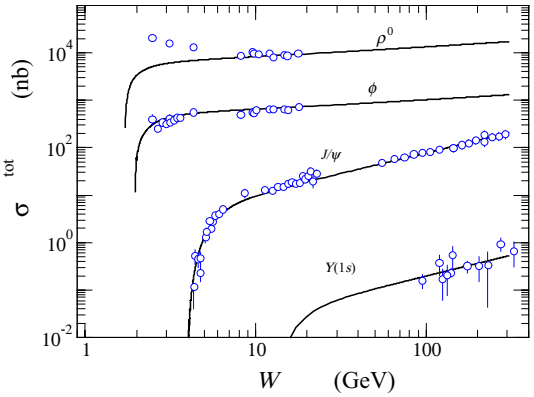

Fig. 6 Total cross-section versus beam energy W for $\gamma p \to (\rho^0, \phi, J/\Psi, \Upsilon(1\,s))p$ [54] using the DL Pomeron model [33]. Figure is taken from Ref. [55]

$$F_N(t) = \frac{4M_N^2 - 2.8t}{(4M_N^2 - t)(1 - t/0.71)^2}. \tag{10}$$

The Regge phenomenology is involved in the propagator $G_{\mathbb{P}}(s,t)$ in Eq. (7):

$$G_{\mathbb{P}}(s,t) = \left(\frac{s}{s_0}\right)^{\alpha_P(t)-1}\exp\left\{-\frac{i\pi}{2}\left[\alpha_P(t) - 1\right]\right\}, \tag{11}$$

where $\alpha_P(t) = \alpha_0 + \alpha_P' t$ is the Pomeron trajectory. The model parameters are determined by fitting to the cross-section data of ρ^0, ω, and ϕ photoproduction:

$$\begin{aligned}&\mu_0 = 1.1\ \text{GeV}^2,\ \ \beta_q = 2.07\ \text{GeV}^{-1},\ \ \beta_s = 1.39\ \text{GeV}^{-1},\\ &\alpha_0 = 1.08,\ \ \alpha_P' = 1/s_0 = 0.25\ \text{GeV}^{-2}.\end{aligned} \tag{12}$$

For the heavy quark system, some values are rather different from the light quark (u, d, s) system, that is, $\beta_c = 0.323\,\text{GeV}^{-1}$ and $\beta_b = 0.452\,\text{GeV}^{-1}$ for J/ψ and $\Upsilon(1s)$ photoproduction, respectively, and $\alpha_0 = 1.25$ [53].

The total cross-sections for ρ^0, ϕ, J/ψ, and $\Upsilon(1s)$ production are depicted in Fig. 6 as a result of Pomeron exchange and turn out to be in good agreement with the experimental data at high energies [54, 55]. Meanwhile, that for ρ^0 (and possibly ω) production implies the need for meson exchanges of Fig. 5b at low energies. Also the N^* contributions could be important in the s channel as indicated from the values of their branching ratios for decays into ρN and ωN (see Table 1) [56–61]. We see that the branching ratios of N^* to ρN and ωN are much larger than those to $K^*\Lambda$. Most of the values $\text{Br}_{N^*\to\omega N}$ are extracted by including the BnGa partial wave analysis [59]. Note that none of the decays $N^* \to \phi N$ is firmly observed experimentally.

A prominent feature that emerged in $\gamma p \to \phi p$ is that a bump structure is observed for $d\sigma/dt$ at $t = t_{min}$ around

$E_\gamma \sim 2$ GeV as shown in Fig. 7. It is reported by the LEPS Collaboration [25] and confirmed by Refs. [27–29]. The Pomeron plus (π^0, η) meson exchange model (green solid curve) [62] cannot explain this local structure. References [63–65] attribute it to a postulated spin-3/2 N^* resonance with $M_{N^*} \approx 2.1$ GeV and $\Gamma_{N^*} \approx 500$ MeV. Interestingly, the CLAS Collaboration [26–28] has found that the structure persists only in the forward angles and vanishes around $\cos\theta \approx 0.8$, where $\cos\theta$ is the ϕ-meson scattering angle in the c.m. frame. Thus the interpretation of it as excitation of resonances [63–65] seems unlikely although not totally impossible.

Meanwhile, the bump structure is interpreted as the coupled-channel effects between the ϕp and $K^+\Lambda(1520)$ channels [66–68]. However, the similarity between the charged $(\phi \to K^+K^-)$ and neutral modes $(\phi \to K^0_S K^0_L)$ for $\gamma p \to \phi p$ [27, 28] implies that the rescattering effect and the interference are marginal. Moreover, it is confirmed by the LEPS Collaboration [30] that the $E_\gamma \sim 2.0$ GeV structure is regardless of the ϕ-$\Lambda(1520)$ interference effect in the $\gamma p \to K^+K^-p$ reaction.

Although the meson and N^* contributions are expected to be small in ϕ photoproduction due to the OZI rule [34–36], their contributions turn out to be nonnegligible for describing the abundant CLAS data [26–28] on the wide scattering angles of the differential cross-sections and spin-density matrices [55, 69]. Proton exchange is responsible for the backward angle data. Two N^* resonances account for the two bumplike structures around $\sqrt{s} \sim 2.1$ and 2.3 GeV at backward angles regardless of the much larger structure illustrated in Fig. 7 [55, 69]. Keeping these in mind, more rigorous theoretical studies are called for a better understanding of the bump structure. It is also found that the effects of the final state interaction (FSI) are negligible in Ref. [55] where the gluon exchange, direct ϕN couplings, and the box diagrams arising from the couplings with πN, ρN, $K\Lambda$, and $K\Sigma$ channels are included as for the FSI terms.

The possible existence of the hidden-strangeness pentaquark state $P_s^+[uuds\bar{s}]$ is discussed in Ref. [70] as its charmed partner, i.e., three exotic charmonium-like states $P_c^+(4312)$, $P_c^+(4440)$, and $P_c^+(4457)$, are observed by the LHCb Collaboration [71, 72]. $P_s^+(P_c^+)$ can be examined in the s-channel diagram in the $\gamma p \to \phi(J/\psi)p$ reaction as displayed in Fig. 8.

The total cross-section for $\gamma p \to J/\psi p$ is depicted in Fig. 9. The GlueX data in Hall D at the JLab [31] and previous data [73, 74] are compared with theoretical models [75–77]. The two- and three-hard-gluon exchange processes based on perturbative QCD and effective heavy quark field theory are studied in Ref. [76]. The GlueX data do not consistent with the narrow peak predicted by the JPAC model [77] at $E_\gamma \simeq 10$ GeV and can be used to constrain the upper limits on the branching fraction of the pentaquark P_c^+ states. Note that the first measurements of $d\sigma/dt$ in the range of 9.1 GeV $\leq E_\gamma \leq$ 10.6 GeV are recently reported by the Hall C experiment at the JLab [32] which can give us a hint on the existence of P_c^+ via $\gamma p \to J/\psi p$.

Following the same line of reasoning, a new proposal is recently submitted to the J-PARC facility to investigate the

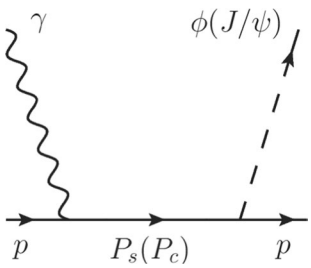

Fig. 8 Pentaquark $P_s(P_c)$ exchange in s channel diagram in the $\gamma p \to \phi(J/\psi)p$ reaction

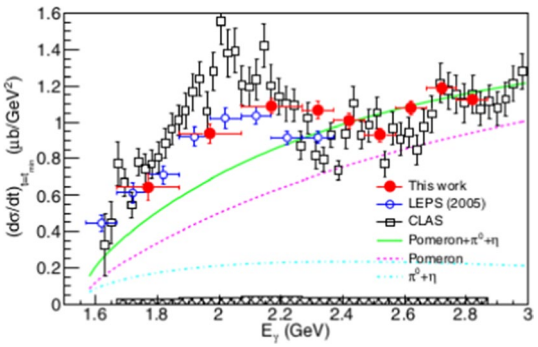

Fig. 7 Differential cross-section $d\sigma/dt$ versus beam energy E_γ at $t = t_{min}$ for $\gamma p \to \phi p$. The blue empty circle [25] and the red full circle [29] are from the LEPS Collaboration. The black empty square [27, 28] is from the CLAS Collaboration. Figure is taken from Ref. [29]

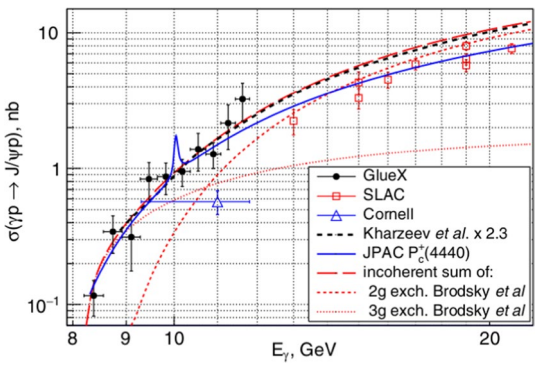

Fig. 9 Total cross-section versus beam energy E_γ for $\gamma p \to J/\psi p$. The GlueX data [31] are compared with the previous SLAC [73] and Cornell [74] data. The theoretical predictions are from Ref. [75] (black dashed), Ref. [77] (blue solid), and Ref. [76] (red dashed). Figure is taken from Ref. [31]

$\pi^- p \to \phi n$ reaction [78] which offers an ideal opportunity for observing s-channel resonances, especially the hidden-strangeness pentaquark P_s state. Or in view of the puzzled situation related to the interpretation of the bump structure illustrated in Fig. 7, the simultaneous study of $\pi^- p \to \phi n$ to $\gamma p \to \phi p$ will be very valuable to understand the underlying mechanism.

3 Electroproduction of vector mesons

The schematic representation of the vector-meson electroproduction $ep \to eVp$ is displayed in Fig. 10 which consists of the (a) electron scattering plane, (b) hadronic production plane, and (c) decay plane. In the hadron production plane, $\gamma^* p \to V(\rho^0, \omega, \phi)p$, the cross-section dependence on the angle Φ is separated in transverse (T), longitudinal (L), and interference (TT, LT) parts as

$$\frac{d\sigma}{d\Phi} = \frac{1}{2\pi}(\sigma + \varepsilon\sigma_{TT}\cos 2\Phi + \sqrt{2\varepsilon(1+\varepsilon)}\sigma_{LT}\cos\Phi), \quad (13)$$

where $\sigma = \sigma_T + \varepsilon\sigma_L$. ε characterizes the degree of longitudinal polarization of the virtual photon

$$\varepsilon = \left[1 + \frac{2\mathbf{k}^2}{Q^2}\tan^2\frac{\theta_e}{2}\right]^{-1}, \quad (14)$$

where $\mathbf{k}$ is the three-momentum of the initial particles.

Figure 11 illustrates the kinematical range covered by the vector-meson electroproduction experiments. Here $x_B = Q^2/2M_p\nu$ denotes for the usual Bjorken variable where $\nu = E_e - E_{e'}$ is the energy transfer in laboratory frame. The HERA experiment at the ZEUS and H1 Collaborations is performed at high ranges of W and Q^2 (e.g., $40 \le W \le 130$ GeV and $1 \le Q^2 \le 15$ GeV^2 at H1 [79])

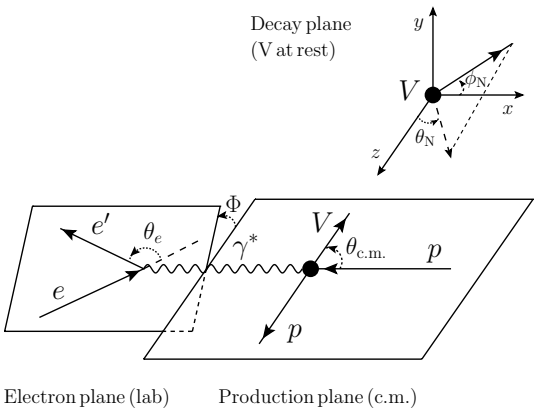

Fig. 10 Reference frames and relevant variables for the description of $ep \to eVp$: **a** electron scattering plane ($ee'\gamma^*$) defined in laboratory frame, **b** hadron production plane ($\gamma^* Vp$) in $\gamma^* p$ c.m. frame, and **c** decay plane ($V \to$ decay) in V rest frame

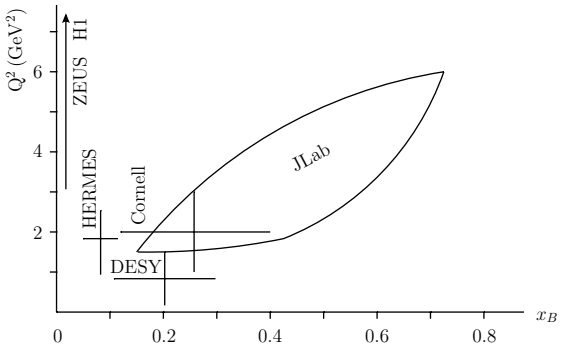

Fig. 11 Kinematical range covered by the vector-meson electroproduction experiments. The lines indicate the total coverage in Q^2 and x_B [41]

and thus the GPD formulation is most applicable. Meanwhile, the old experiments at the Cornell group [44] and HERMES Collaboration at DESY [39, 40, 42, 43] are carried out at low ranges of W and Q^2 (e.g., $3.0 \le W \le 6.3$ GeV and $0.5 \le Q^2 \le 7.0$ GeV^2 at HERMES [39]) such that a hadronic Regge model is more successful.

The CLAS experiment at the JLab is more interesting. It aims to reach the highest achievable Q^2 values in the valence-quark region [37, 38, 41, 45–47]. Thus we can test which of the two descriptions applies in the considered kinematical domain: hadronic or partonic descriptions, i.e., t-channel meson exchange (Fig. 1a) or handbag diagram (Fig. 1b). For example, the so-called "JML" Regge model, developed by Laget et al. [80, 81], is widely used to describe the meson exchange diagram. In a similar approach, Ref. [82] has investigated the $\gamma^* p \to \phi p$ reaction. A hadronic model is used in Ref. [83] to study the $ep \to e' J/\psi p$ reaction focusing the role of the pentaquark state $P_c(4312)$ in the s channel. On the other hand, the "VGG" GPD-based model, developed by M. Vanderhaeghen and collaborators [84–87], is well known to describe the hard scattering mechanism.

The measurements of the interference terms σ_{TT} and σ_{LT} in Eq. (13) are of particular importance because they are relevant to the s-channel helicity conservation (SCHC). If the vector meson is produced with the same helicity as the γ^*, SCHC is said to hold. Then, σ_{TT} and σ_{LT} vanish by definition. SCHC can be also tested by studying the spin-density matrices and decay angular distributions, e.g., $\rho^0_{00} = 0$ and $\rho^4_{00} = 1$ if SCHC applies. More data from the upgraded 12 GeV JLab experiment [88] are necessary to reach a firm conclusion concerning SCHC for $\gamma^* p \to V(\rho^0, \omega, \phi)p$ and will need further exploration.

Meanwhile, a GPD-based model is also accessible to the processes of the deeply virtual spin-0 meson electroproduction [89–92] and the deeply virtual compton scattering (DVCS) [93–96]. In Ref. [89], the first high Q^2 measurements and complete angular distributions for exclusive π^+

electroproduction on protons in the N^* resonance region are reported. In Ref. [90], for the first time target and double spin asymmetries from deeply virtual π^0 meson production are extracted over a wide range of Q^2, x_B, and $-t$. In Ref. [92], light-front time-ordered amplitudes are investigated in the virtual scalar meson production process in (1+1) dimensions using the scalar field model extended from the conventional Wick–Cutkosky model. The unpolarized and beam-polarized fourfold cross-sections ($d^3\sigma/dQ^2dx_Bdtd\phi$) are measured for the DVCS over the widest phase space ever covered in the valence-quark region in Ref. [93], revealing from the experiment a first tomographic image of the nucleon.

4 Summary

Production of vector mesons via various scattering processes opens new channels to identify high-mass baryon resonances and to investigate their properties. Especially, there has been significant progress on the exclusive photoproduction of vector mesons over the last decade. Accurate and abundant data on the cross-sections, spin density matrices, and spin polarization observables are produced from the CLAS, GlueX, and LEPS Collaborations for K^* [11, 12], ρ^0 [21], ω [23, 24], ϕ [26–30], and J/ψ [31, 32] productions.

Theoretically, an effective Lagrangian approach and a Regge model are used intensively in a single channel analysis. The BnGa partial wave analysis is used to describe $K^*\Lambda$ [12] and ωN [59] photoproduction. Since Pomeron exchange is absent in photoproduction of strange mesons, its main production mechanisms is distinguished from that of light vector mesons. We review the bump structure observed at forward angles in ϕ photoproduction [25, 27–29] in some detail. The possible existence of the hidden-strangeness P_s^+ and hidden-charm P_c^+ pentaquark states is discussed via ϕ and J/ψ photoproduction, respectively.

We also review the exclusive electroproduction of vector mesons and compare two different theoretical models. A "JML" Regge model [80, 81] is designed to describe the t-channel meson exchange diagram, whereas a "VGG" GPD-based model [84–87] is adequate for the hard scattering mechanism. The upcoming data from the CLAS [88] are particularly promising because they cover wide kinematical ranges of Q^2 and x_B and thus provide a unique opportunity to test the two models.

Acknowledgements This work was supported by Basic Science Research Program through the National Research Foundation of Korea (NRF) funded by the Ministry of Education (Grants No. NRF-2021R1A6A1A03043957 and NRF-2022R1I1A1A01054390).

References

1. R.L. Workman, Particle Data Group et al., Prog. Theor. Exp. Phys. **2022**, 083C01 (2022)
2. S. Capstick, W. Roberts, Phys. Rev. D **58**, 074011 (1998)
3. Y. Oh, H. Kim, Phys. Rev. C **73**, 065202 (2006)
4. Y. Oh, H. Kim, Phys. Rev. C **74**, 015208 (2006)
5. S.H. Kim, S.I. Nam, Y. Oh, H.C. Kim, Phys. Rev. D **84**, 114023 (2011)
6. S.H. Kim, A. Hosaka, H.C. Kim, Phys. Rev. D **90**, 014021 (2014)
7. S.H. Kim, S.I. Nam, A. Hosaka, H.C. Kim, Phys. Rev. D **88**, 054012 (2013)
8. B.G. Yu, Y. Oh, K.J. Kong, Phys. Rev. D **95**, 074034 (2017)
9. I. Hleiqawi, CLAS Collaboration et al., Phys. Rev. C **75**, 042201 (2007)
10. I. Hleiqawi, CLAS Collaboration et al., Phys. Rev. C **76**, 039905(E) (2007)
11. W. Tang, CLAS Collaboration et al., Phys. Rev. C **87**, 065204 (2013)
12. A.V. Anisovich, CLAS Collaboration et al., Phys. Lett. B **771**, 142 (2017)
13. M. Nanova, CBELSA/TAPS Collaboration et al., Eur. Phys. J. A **35**, 333 (2008)
14. S.H. Hwang, LEPS Collaboration et al., Phys. Rev. Lett. **108**, 092001 (2012)
15. M.E. McCracken, CLAS Collaboration et al., Phys. Rev. C **81**, 025201 (2010)
16. K. Moriya, CLAS Collaboration et al., Phys. Rev. C **88**, 045201 (2013)
17. S.H. Kim, S.I. Nam, D. Jido, H.C. Kim, Phys. Rev. D **96**, 014003 (2017)
18. S.H. Kim, H.C. Kim, Phys. Lett. B **786**, 156 (2018)
19. S. H. Kim, K. P. Khemchandani, A. Martinez Torres, S. I. Nam, A. Hosaka, Phys. Rev. D **103**, 114017 (2021)
20. C. Wu, J. Barth, W. Braun, J. Ernst, K.H. Glander, J. Hannappel, N. Jopen, H. Kalinowsky, F.J. Klein, F. Klein et al., Eur. Phys. J. A **23**, 317 (2005)
21. E. Golovatch, CLAS Collaboration et al., Phys. Lett. B **788**, 371 (2019)
22. M. Williams, CLAS Collaboration et al., Phys. Rev. C **80**, 065208 (2009)
23. A. Wilson, CBELSA/TAPS Collaboration et al., Phys. Lett. B **749**, 407 (2015)
24. P. Roy, CLAS Collaboration et al., Phys. Rev. Lett. **122**, 162301 (2019)
25. T. Mibe, LEPS Collaboration et al., Phys. Rev. Lett. **95**, 182001 (2005)
26. H. Seraydaryan, CLAS Collaboration et al., Phys. Rev. C **89**, 055206 (2014)
27. B. Dey, CLAS Collaboration et al., Phys. Rev. C **89**, 055208 (2014)
28. B. Dey, CLAS Collaboration et al., Phys. Rev. C **90**, 019901(E) (2014)
29. K. Mizutani, LEPS Collaboration et al., Phys. Rev. C **96**, 062201 (2017)
30. S.Y. Ryu, LEPS Collaboration et al., Phys. Rev. Lett. **116**, 232001 (2016)
31. A. Ali, GlueX Collaboration et al., Phys. Rev. Lett. **123**, 072001 (2019)
32. B. Duran, Z. E. Meziani, S. Joosten, M. K. Jones, S. Prasad, C. Peng, W. Armstrong, H. Atac, E. Chudakov, H. Bhatt, et al.. arXiv:2207.05212 [nucl-ex]
33. A. Donnachie et al., *Pomeron Physics and QCD* (Cambridge University Press, Cambridge, England, 2002)
34. S. Okubo, Phys. Lett. **5**, 165 (1963)

35. G. Zweig, CERN Reports, CERN-TH-401 and CERN-TH-412 (1964)
36. J. Iizuka, Prog. Theor. Phys. Suppl. **37**, 21 (1966)
37. C. Hadjidakis, CLAS Collaboration et al., Phys. Lett. B **605**, 256 (2005)
38. S.A. Morrow, CLAS Collaboration et al., Eur. Phys. J. A **39**, 5 (2009)
39. A. Airapetian, HERMES Collaboration et al., Eur. Phys. J. C **71**, 1609 (2011)
40. A. Airapetian, HERMES Collaboration et al., Eur. Phys. J. C **77**, 378 (2017)
41. L. Morand, CLAS Collaboration et al., Eur. Phys. J. A **24**, 445 (2005)
42. A. Airapetian, HERMES Collaboration et al., Eur. Phys. J. C **74**, 3110 (2014)
43. A. Airapetian, HERMES Collaboration et al., Eur. Phys. J. C **76**, 162 (E) (2016)
44. R.L. Dixon, R. Galik, M. Herzlinger, S.D. Holmes, D. Larson, F.M. Pipkin, S. Raither, A. Silverman, R.L. Wagner, Phys. Rev. Lett. **39**, 516 (1977)
45. K. Lukashin, CLAS Collaboration et al., Phys. Rev. C **63**, 065205 (2001)
46. K. Lukashin, CLAS Collaboration et al., Phys. Rev. C **64**, 059901 (E) (2001)
47. J.P. Santoro, CLAS Collaboration et al., Phys. Rev. C **78**, 025210 (2008)
48. V.G.J. Stoks, Th.A. Rijken, Phys. Rev. C **59**, 3009 (1999)
49. Th.A. Rijken, V.G.J. Stoks, Y. Yamamoto, Phys. Rev. C **59**, 21 (1999)
50. K. Schilling, P. Seyboth, G.E. Wolf, Nucl. Phys. B **15**, 397 (1970)
51. K. Schilling, P. Seyboth, G. E. Wolf, Nucl. Phys. B **18**, 332 (E) (1970)
52. M.A. Pichowsky, T.S.H. Lee, Phys. Rev. D **56**, 1644 (1997)
53. J.J. Wu, T.S.H. Lee, Phys. Rev. C **86**, 065203 (2012)
54. Durham Database. https://www.hepdata.net/
55. S.H. Kim, T.S.H. Lee, S.I. Nam, Y. Oh, Phys. Rev. C **104**, 045202 (2021)
56. Y. Oh, T.S.H. Lee, Phys. Rev. C **69**, 025201 (2004)
57. Y. Oh, T.S.H. Lee, Phys. Rev. C **66**, 045201 (2002)
58. A.I. Titov, T.S.H. Lee, Phys. Rev. C **66**, 015204 (2002)
59. I. Denisenko, A.V. Anisovich, V. Crede, H. Eberhardt, E. Klempt, V.A. Nikonov, A.V. Sarantsev, H. Schmieden, U. Thoma, A. Wilson, Phys. Lett. B **755**, 97 (2016)
60. N.C. Wei, F. Huang, K. Nakayama, D.M. Li, Phys. Rev. D **100**, 114026 (2019)
61. B.G. Yu, K.J. Kong, Phys. Rev. D **99**, 014031 (2019)
62. A.I. Titov, T.S.H. Lee, Phys. Rev. C **67**, 065205 (2003)
63. A. Kiswandhi, J.J. Xie, S.N. Yang, Phys. Lett. B **691**, 214 (2010)
64. A. Kiswandhi, S.N. Yang, Phys. Rev. C **86**, 015203 (2012)
65. A. Kiswandhi, S. N. Yang, Phys. Rev. C **86**, 019904 (E) (2012)
66. S. Ozaki, A. Hosaka, H. Nagahiro, O. Scholten, Phys. Rev. C **80**, 035201 (2009)
67. S. Ozaki, A. Hosaka, H. Nagahiro, O. Scholten, Phys. Rev. C **81**, 059901 (E) (2010)
68. H. Y. Ryu, A. I. Titov, A. Hosaka, H.-C. Kim, Prog. Theor. Exp. Phys. **2014**, 023D03 (2014)
69. S.H. Kim, S.I. Nam, Phys. Rev. C **100**, 065208 (2019)
70. R.F. Lebed, Phys. Rev. D **92**, 114030 (2015)
71. R. Aaij, LHCb Collaboration et al., Phys. Rev. Lett. **115**, 072001 (2015)
72. R. Aaij, LHCb Collaboration et al., Phys. Rev. Lett. **122**, 222001 (2019)
73. U. Camerini, J.G. Learned, R. Prepost, C.M. Spencer, D.E. Wiser, W. Ash, R.L. Anderson, D. Ritson, D. Sherden, C.K. Sinclair, Phys. Rev. Lett. **35**, 483 (1975)
74. L.B. Leipuner, R.C. Larsen, R.K. Adair, P.D. Bergey, A.B. Carter, D.M. Grannan, H. Kasha, R.G. Kellogg, M.J. Lauterbach, Phys. Rev. Lett. **35**, 1613 (1975)
75. D. Kharzeev, H. Satz, A. Syamtomov, G. Zinovev, Nucl. Phys. A **661**, 568 (1999)
76. S.J. Brodsky, E. Chudakov, P. Hoyer, J.M. Laget, Phys. Lett. B **498**, 23 (2001)
77. A. N. Hiller Blin, C. Fernández-Ramírez, A. Jackura, V. Mathieu, V. I. Mokeev, A. Pilloni, A. P. Szczepaniak, Phys. Rev. D **94**, 034002 (2016)
78. T. Ishikawa, et al., Pion-induced phi-meson production on the proton, Proposal for the J-PARC 30-GeV Proton Synchrotron (2022)
79. C. Adloff, H1 Collaboration et al., Phys. Lett. B **483**, 360 (2000)
80. J.M. Laget, Phys. Lett. B **489**, 313–318 (2000)
81. J.M. Laget, Phys. Rev. D **70**, 054023 (2004)
82. S.H. Kim, Si. Nam, Phys. Rev. C **101**, 065201 (2020)
83. I.W. Park, S. Cho, Y. Kim, S.H. Lee, Phys. Rev. D **105**, 114023 (2022)
84. M. Vanderhaeghen, P.A.M. Guichon, M. Guidal, Phys. Rev. Lett. **80**, 5064 (1998)
85. M. Vanderhaeghen, P.A.M. Guichon, M. Guidal, Phys. Rev. D **60**, 094017 (1999)
86. K. Goeke, M.V. Polyakov, M. Vanderhaeghen, Prog. Part. Nucl. Phys. **47**, 401 (2001)
87. M. Guidal, M.V. Polyakov, A.V. Radyushkin, M. Vanderhaeghen, Phys. Rev. D **72**, 054013 (2005)
88. Pre-conceptual design report for the science and experimental equipment for the 12 GeV upgrade of CEBAF. http://www.jlab.org/div_dept/physics_division/pCDR_public/pCDR_final
89. K. Park, CLAS Collaboration et al., Phys. Rev. C **77**, 015208 (2008)
90. A. Kim, H. Avakian, V. Burkert, K. Joo, W. Kim, K..P. Adhikari, Z. Akbar, S. Anefalos Pereira, R.. A. Badui, M. Battaglieri et al., Phys. Lett. B **768**, 168 (2017)
91. C.R. Ji, H.M. Choi, A. Lundeen, B.L.G. Bakker, Phys. Rev. D **99**, 116008 (2019)
92. Y. Choi, H.M. Choi, C.R. Ji, Y. Oh, Phys. Rev. D **103**, 076002 (2021)
93. H.S. Jo, CLAS Collaboration et al., Phys. Rev. Lett. **115**, 212003 (2015)
94. N. Hirlinger Saylor, CLAS Collaboration et al., Phys. Rev. C **98**, 045203 (2018)
95. M. Hattawy, CLAS Collaboration et al., Phys. Rev. Lett. **123**, 032502 (2019)
96. H.S. Jo, New Phys. Sae Mulli **69**, 376–379 (2019)